Journal of Quantitative Spectroscopy & Radiative Transfer 113 (2012) 2197–2204

Contents lists available at SciVerse ScienceDirect

Journal of Quantitative Spectroscopy & Radiative Transfer

journal homepage: www.elsevier.com/locate/jqsrt

High sensitivity cavity ring down spectroscopy of $^{13}C^{16}O_2$ overtone bands near 806 nm

Y. Lu [a], A.-W. Liu [a,*], H. Pan [a], X.-F. Li [a], V.I. Perevalov [b], S.A. Tashkun [b], S.M. Hu [a]

[a] Hefei National Laboratory for Physical Sciences at Microscale, Department of Chemical Physics, University of Science and Technology of China, Hefei 230026, China

[b] Laboratory of Theoretical Spectroscopy, V. E. Zuev Institute of Atmospheric Optics SB, Russian Academy of Science, 1, Akademician Zuev sq., 634021 Tomsk, Russia

ARTICLE INFO

Article history:
Received 17 April 2012
Received in revised form
16 July 2012
Accepted 17 July 2012
Available online 24 July 2012

Keywords:
Cavity ring down spectroscopy
Carbon dioxide
$^{13}C^{16}O_2$
CDSD

ABSTRACT

The absorption spectrum of $^{13}C^{16}O_2$ near 806 nm has been recorded with a continuous-wave cavity ring-down spectrometer. Two cold bands and one associated hot band are observed in this region. The line positions of these bands are determined with an accuracy of 0.003 cm^{-1}. The absolute line intensities have also been retrieved with an estimated accuracy of 4% for majority of the unblended lines. The vibrational transition dipole moment squared values and the empirical Herman–Wallis coefficients are determined for all the three bands. The comparison of the retrieved line positions and intensities to those given in the Carbon Dioxide Spectroscopic Databank shows large deviations in the line intensities of the 10052–00001 band. The effective dipole moment parameters describing the line intensities of $^{13}C^{16}O_2$ near 806 nm are fitted according to the observed line intensities.

1. Introduction

As one of the most important atmospheric molecules, carbon dioxide plays a major role in the greenhouse effect. Carbon dioxide is also the main constituent of the Venus and Mars atmospheres. The weakness of the bands lying near 806 nm is an advantage in probing the atmospheres of these planets since the absorption lines are not saturated even after path lengths of hundreds of kilometers. In particular, the stable carbon and oxygen isotopologue compositions of CO_2 ($\delta^{13}C$ and $\delta^{18}O$) can provide an insight into the determination of the sources and sinks of greenhouse gases [1,2] in atmospheric chemistry, the volcanic gases evaluation in geochemistry, and understanding of the biological activities in biochemistry [3].

The present work is the continuation of a series devoted to the systematic study of the absorption spectrum of carbon dioxide isotopologues corresponding to the overtone bands 10051–00001, 10052–00001 and respective hot bands near 0.8 μm in our laboratory [4]. In this paper the study of the respective $^{13}C^{16}O_2$ bands will be presented. The cold bands 10051–00001 and 10052–00001 of the $^{13}C^{16}O_2$ isotopologue have been studied by Campargue et al. [5] with Intra-Cavity Laser Absorption Spectroscopy (ICLAS). However, the stated accuracy of the obtained ro-vibrational energy levels was limited to 0.01 cm^{-1}. The line intensities have not been determined due to the overlapped atmospheric water absorption in the 760–850 nm region. The high-sensitivity and high-resolution of the cavity ring-down spectroscopy instrument used in this work allow us to measure the line intensities and positions more accurately. The results can be used to refine the effective Hamiltonian and dipole moment parameters for the $^{13}C^{16}O_2$ isotopologue.

* Corresponding author. Tel./fax: +86 551 3607632.
E-mail address: awliu@ustc.edu.cn (A.-W. Liu).

0022-4073/$ - see front matter © 2012 Elsevier Ltd. All rights reserved.
http://dx.doi.org/10.1016/j.jqsrt.2012.07.020

The present paper is organized as follows. In Section 2, we present briefly the experimental procedure and the analysis methodology. Section 3 is devoted to the band-by-band analysis and the global modeling of the line intensities in the considered spectral region. Discussions and conclusions are given in Section 4.

2. Experiment and data reduction

The spectrum of enriched $^{13}C^{16}O_2$ in the 802–812 nm range was measured using a continuous wave cavity ring-down (cw-CRDS) spectrometer. The spectrometer has been described in details in Ref. [6]. The sample absorption coefficient $\alpha(\nu)$ can be retrieved by measuring the ring-down time $\tau(\nu)$ of the transmitted laser beam power:

$$\alpha(\nu)=\frac{1}{c}\left(\frac{1}{\tau(\nu)}-\frac{1}{\tau_0}\right). \quad (1)$$

where c is the speed of light and τ_0 is the ring-down time of empty cavity. The noise-equivalent minimal detectable absorption coefficient α_{min} was about 3×10^{-10} cm^{-1}.

^{13}C enriched carbon dioxide sample with stated ^{13}C atom purity of 99% was purchased from Aldrich. The abundance of $^{13}C^{16}O_2$ was determined at 98.5% with accuracy about 0.2% by a photo-ionization mass spectroscopy (PIMS) experiment measured with a time-of-flight mass spectrometer in the photochemistry end-station of National Synchrotron Radiation Laboratory, Hefei. Two pressures at 80 and 150 Torr were adopted and the spectrum was recorded at room temperature (297 K). The pressure was measured by a manometer with 1000 Torr full-scale range and 0.15% accuracy. The spectrum calibration is based on the readings given by a calibrated lambdameter (Burleigh WA-1500) with 60 MHz accuracy. An overview of the cw-CRDS spectra is presented in Fig. 1, in which three successive enlargements illustrate the R branch of the 11151–01101 hot band.

3. Results

3.1. Transition list

Three bands of $^{13}C^{16}O_2$ were detected near 806 nm. At pressure values over 90 Torr, the collision narrowing and speed dependent effects are not negligible compared to the Doppler and collision broadening effects [7]. In this case the line profile can be better described by either Rautian [8] or Galatry model [9] than by the Voigt profile. In this work, we adopt the "soft" collisional Galatry model. With the Gaussian width fixed at the calculated Doppler width value, other parameters including the line position, intensity, Lorentzian width and Dicke narrowing coefficients were derived using an interactive least squares multi-lines fitting procedure. As illustrated in Fig. 2, the $P(16)$ line in the 10051–00001 band of $^{13}C^{16}O_2$ recorded at 150 Torr is reproduced by the Galatry profile within the experimental uncertainty, the residuals of the fit being at the experimental noise level. The position uncertainty of unblended and not-very-weak lines is estimated to be 0.003 cm^{-1}. The error on the line strength values from the line profile fitting is about 1.5%–2%. Including the pressure uncertainty (0.15%) and the error from the temperature fluctuation (<1%), the accuracy of the line intensities is estimated to be about 4% for majority of the lines. However, the error could exceed 10% for blended or weak lines.

A total of 169 $^{13}C^{16}O_2$ transitions were observed. The full line list is presented in Tables 1–3. The line strength values in the tables have been converted to 100% abundance of $^{13}C^{16}O_2$ and temperature at 296 K.

3.2. Spectroscopic constants of the upper states

Three vibrational bands were rotationally indentified with the help of CDSD [10] databank. The rotational analysis was performed using the standard equation for the vibration–rotation energy levels:

$$F_v(J)=G_v+B_vJ(J+1)-D_vJ^2(J+1)^2+H_vJ^3(J+1)^3, \quad (2)$$

where Gv is the vibrational term value, B_v is the rotational constant, D_v and H_v are centrifugal distortion constants. The spectroscopic parameters for an upper state were fitted directly to the observed line positions of the respective band, and in the case of hot band involving e and f rotational levels, the ee and ff sub band were considered independently. The lower state rotational constants were constrained to their literature values [11]. The spectroscopic parameters retrieved from the fitting are presented in Table 4. The rms values of the (obs.−calc.) deviations are generally 1×10^{-3} cm^{-1} which is consistent with the experimental accuracy. The corresponding spectroscopic parameters reported in literatures are also presented in italics in Table 4.

3.3. Vibrational transition dipole moment squared, and Herman–Wallis factor

The line intensity $S(T_0)$ in cm^{-1}/(cm^{-2} molecule) at the standard temperature T_0=296 K can be given by the following equation:

$$S(T_0)=\frac{1}{4\pi\varepsilon_0}\frac{8\pi^3\nu_0}{3hcQ(T_0)}|R|^2L(J,l)e^{-hcE''/kT_0}\left[1-e^{-hc\nu_0/kT_0}\right] \quad (3)$$

In Eq. (3), $1/4\pi\varepsilon_0=10^{-36}$ erg cm^3 D^{-2}; h is the Planck constant; c is the speed of light; ν_0 is the transition wavenumber in cm^{-1}; $Q(T_0)$ is the total partition function at temperature T_0; $L(J,l)$ is the Hönl–London factor; J is the lower state rotational quantum number; l is the quantum number of the projection of the vibrational angular momentum on the molecular axis z; E'' is the lower level energy in cm^{-1}; and k is the Boltzmann constant.

For the parallel bands, the Hönl–London factor $L(J,l)$ is equal to $|m|$, where m is $-J$ for P branch transitions, and $J+1$ for R branch. For the isolated vibrational states of a linear molecule, the rotational dependence of the transition dipole moment squared can be expressed as

$$|R|^2=|R_0|^2F(m). \quad (4)$$

where $|R_0|^2$ is the vibrational transition dipole moment squared, $F(m)$ is the empirical Herman–Wallis factor

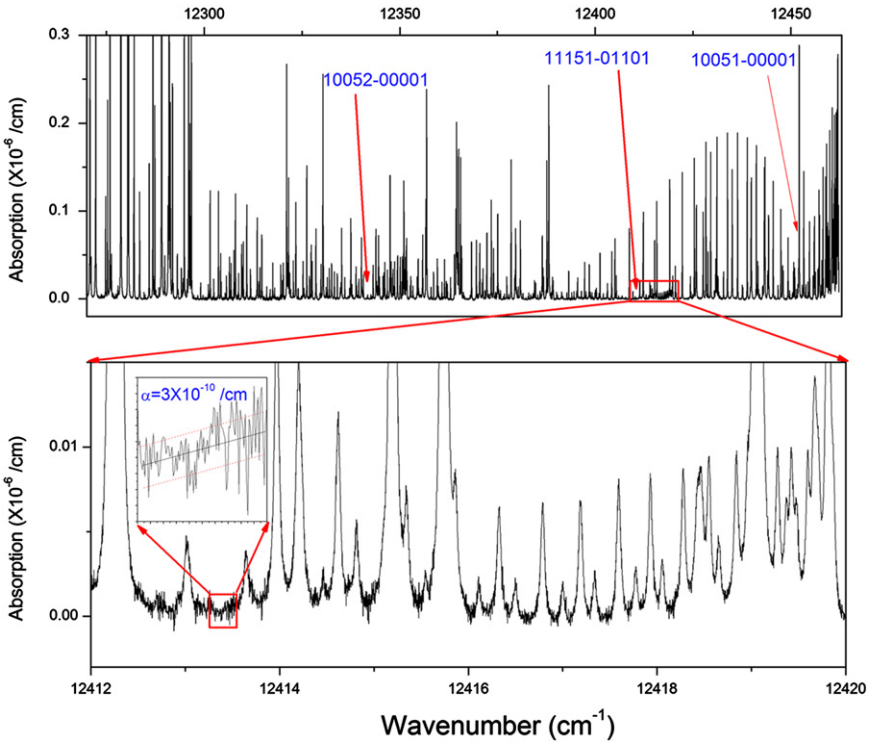

Fig. 1. Overview of the CRDS spectrum of ^{13}C enriched carbon dioxide around 806 nm. The sample pressure is 150 Torr. The noise equivalent absorption in the insert is about 3×10^{-10} cm^{-1}.

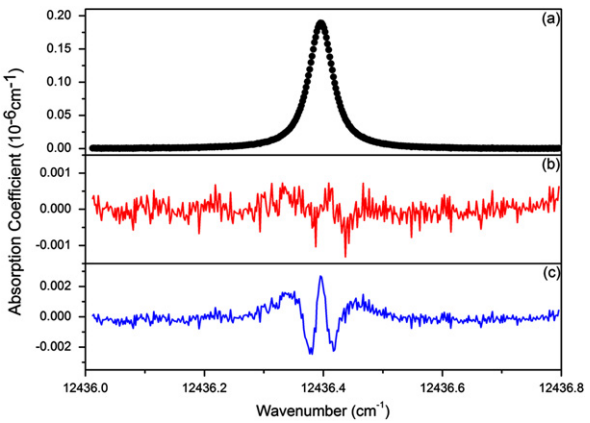

Fig. 2. The $P(16)$ line in the 10051–00001 cold band of $^{13}C^{16}O_2$ recorded at 150 Torr. (a) Observed CRDS spectrum. (b) and (c) are the fitting residuals using the Galatry and Voigt profiles, respectively. The Gaussian width was fixed at the Doppler width value in all the fittings.

which can be interpreted with.

$$F(m)=(1+A_1m+A_2m^2)^2, \quad (5)$$

where A_1 and A_2 are the Herman–Wallis coefficients.

We have retrieved the vibrational transition dipole moment squared and the Herman–Wallis coefficients by the fitting to the line intensities corresponding to unblended transitions. The obtained values are given in Table 4. The line intensities calculated with this set of Herman–Wallis coefficients are given in Tables 1 and 2 for the 10051–00001 and 10052–00001 cold bands, respectively. The blended lines marked with '*' in the tables have been excluded from the fit. In Fig. 3, the plot of the transition dipole moment squared versus rotational quantum number m is given for two cold bands.

3.4. Effective dipole moment parameters

In this subsection we present the results of the modeling of the line intensities of the observed bands within the framework of the method of effective operators. Contrary to the modeling performed in the preceding section, this modeling allows to perform the extrapolation calculations of the line intensities of the hot bands belonging to the same series of transitions. In our case it is the $P=17$ series of transitions, where P is the polyad number ($P=2V_1+V_2+3V_3$). The vibrational energy levels in the case of carbon dioxide molecule are grouped into polyads due to the approximate relations between the harmonic frequencies [12,13]

$$\omega_1\approx2\omega_2, \quad \omega_3\approx3\omega_2, \quad (6)$$

The theoretical approach used for the line intensity calculations is only briefly given here for the reader's convenience. More details can be found in our previous studies [14–16]. A global effective Hamiltonian describing the line positions of carbon dioxide is formulated to be block diagonal for the polyads of the interacting vibrational states. And all resonance interactions between vibrational states belonging to the same polyad are taken into account up to the sixth order effective Hamiltonian expansion.

Within the framework of the effective operators approach, the square of the transition dipole moment of a vibration–rotation transition $P'N'J'\varepsilon' \leftarrow P\,N\,J\varepsilon$ is given by [14–16].

$$W_{P'N'J'\varepsilon'\leftarrow PNJ\varepsilon} = (2J+1)\left|\sum_{V_1V_2\ell_2V_3}\ \sum_{\substack{2\Delta V_1+\Delta V_2+3\Delta V_3=\Delta P\\ \Delta\ell_2=0,\pm1,\pm2,\ldots}} {}^{J}C_{PN\varepsilon}^{V_1V_2\ell_2V_3}\,{}^{J'}C^{V_1+\Delta V_1V_2+\Delta V_2\ell_2+\Delta\ell_2V_3+\Delta V_3}\,M_{\Delta V}^{|\Delta\ell_2|}\right.$$
$$\left.\times\sqrt{f_{\Delta V}^{\Delta\ell_2}(V,\ell_2)(1+\delta_{\ell_2,0}+\delta_{\ell_2',0}-2\delta_{\ell_2,0}\delta_{\ell_2',0})}\quad {}^{P'N'\varepsilon'}\Phi_{\Delta J,\Delta\ell_2}(J,\ell_2)\right|^2 \tag{7}$$

here $\delta_{i,j}$ is the Kronecker symbol and ${}^{J}C_{PN\varepsilon}^{V_1V_2\ell_2V_3}$ stands for the expansion coefficient determining the eigenfunction of the lower state

$$\psi_{PNJ\varepsilon}^{eff} = \sum_{\substack{2V_1+V_2+3V_3=P\\ \ell_2}} {}^{J}C_{PN\varepsilon}^{V_1\,V_2\,\ell_2\,V_3}\,|V_1V_2|\ell_2|V_3J\varepsilon\rangle, \tag{8}$$

The summation runs over all states within the polyad involved. The definition of the Wang-type basis functions $V_1V_2|\ell_2|V_3J\varepsilon\rangle$ has been given in Ref. [14]. In the same way, ${}^{J'}C_{P'N'\varepsilon'}^{V_1\,V_2\,\ell_2\,V_3}$ stands for the expansion coefficient within the upper-state polyad. The functions $\Phi_{\Delta J\Delta\ell_2}(J,\ell_2)$ for $\Delta\ell_2=0,\pm1$ are equal to the Clebsh–Gordon coefficients $(1\Delta\ell_2J\ell_2|(J+\Delta J)(\ell_2+\Delta\ell_2))$, related to the Hönl–London factors by the equation

$$\left|(1\Delta\ell_2J\ell_2|(J+\Delta J)(\ell_2+\Delta\ell_2))\right|^2 = \frac{L_{\Delta J}^{\Delta\ell_2}}{2J+1}, \tag{9}$$

The $f_{\Delta V}^{\Delta\ell_2}(V,\ell_2)$ functions are listed in Table 1 of Ref. [14] for small values of the quantum number differences ΔV. We do not present the Herman–Wallis type functions [14–17] in Eq.(7) because they do not give remarkable difference in this study. In this approximation, the line

Table 1
Line parameters of the 10,051–00,001 band of $^{13}C^{16}O_2$.

J	P(J)					R(J)				
	Position cm^{-1}	$S_{mea}\times10^{27}$ cm^{-1}/(cm^{-2} mole)	$Pos_{Mea.}-Pos_{Cal}$ $\times10^{-3}$ cm^{-1}	%[a]	$\lvert R\rvert^2_{mea}\times10^{11}$ $Debye^2$	Position cm^{-1}	$S_{mea}\times10^{27}$ cm^{-1}/(cm^{-2} mole)	$Pos_{Mea.}-Pos_{Cal}$ $\times10^{-3}$ cm^{-1}	%	$\lvert R\rvert^2_{mea}\times10^{11}$ $Debye^2$
2	12451.0033	0.58	0.2	−2.6	1.63					
4	12449.2867	1.12	−0.7	−3.4	1.62	12456.0342	1.45	1.1	0.7	1.68
6	12447.4475	1.60	−0.5	−3.4	1.62	12457.1927	1.94	1.1	0.1	1.67
8	12445.4841	2.11	−0.8	1.3	1.69	12458.2259	2.31	−0.4	−1.7	1.64
10	12443.3977	2.36	−0.4	−2.7	1.62	12459.1372	2.63	0.1	−1.6	1.64
12	12441.1870	2.65	−0.7	−0.3	1.66	12459.9251	2.88	1.1	−0.1	1.66
14	12438.8525	2.68	−1.3	−4.2	1.60	12460.5882	2.98	1.1	−0.5	1.65
16	12436.3959	2.83	−0.5	−0.5	1.65	12461.1256	3.08	−0.8	2.0	1.69
18	12433.8148	2.80	−0.7	0.5	1.67	12461.5416	3.08	−0.3	4.4	1.73
20	12431.1106	2.69	−0.6	1.0	1.67	12461.8342	2.95	0.6	4.9	1.74
22	12428.2846	2.51	0.9	0.9	1.67	12462.0024	2.42	0.9	−7.7	1.53
24	12425.3327	2.24	−0.4	−0.8	1.63	12462.0456*	2.02	−0.1	−17.0	1.40
26	12422.2591	2.02	−0.1	0.2	1.65	12461.9677*	2.53	1.4	17.2	1.98
28	12419.0615	1.87	−0.9	6.3	1.75	12461.7634	1.84	0.2	0.9	1.65
30	12415.7419	1.49	−0.8	−0.6	1.62	12461.4382	1.51	1.6	−2.9	1.58
32	12412.3002	1.32	0.1	5.3	1.72	12460.9861	1.31	−0.4	0.9	1.64
34	12408.7361	1.02	1.3	−0.5	1.61	12460.4133	1.08	0.3	1.7	1.64
36	12405.0466	0.89	−0.3	6.8	1.73	12459.7153	0.86	−0.6	0.5	1.62
38	12401.2377	6.76	1.1	3.1	1.66					
40	12397.3041	0.50	0.1	−1.7	1.57	12457.9531	0.53	0.9	1.2	1.62
42	12393.2502	0.39	1.1	−0.2	1.59	12456.8846	0.39	−1.1	−2.3	1.55
44	12389.0715*	0.35	−0.8	17.0	1.91	12455.6954	0.30	−0.7	−0.4	1.58
46	12384.7744*	0.24	1.0	12.0	1.79	12454.3827	0.22	−0.8	−0.5	1.57
48	12380.3523*	0.17	−0.5	10.8	1.76	12452.9468	0.17	−1.4	5.7	1.66
50	12375.8103	0.10	−0.2	−7.1	1.46	12451.3889	0.11	−1.2	−7.4	1.45
52	12371.1479*	0.066	1.1	−16.6	1.33	12449.7092*	0.11	−0.1	25.1	2.07
54	12366.3610*	0.059	−0.9	9.5	1.70					
56	12361.4599*	0.053	4.1	32.6	2.28	12445.9816*	0.040	1.1	9.1	1.68
58	12356.4267*	0.029	−2.1	17.1	1.84	12443.9335*	0.029	0.7	15.3	1.79

[a] Intensity ratio of the difference and measured intensity; the blended lines are marked with '*'.

Table 2
Line parameters of the 10052–00001 band of $^{13}C^{16}O_2$.

J	P(J)					R(J)				
	Position cm^{-1}	$S_{mea} \times 10^{28}$ $cm^{-1}/(cm^{-2}$ mole)	$Pos_{Mea.}-Pos_{Cal}$ $\times 10^{-3}$ cm^{-1}	%[a]	$\lvert R\rvert^2_{obs} \times 10^{12}$ Debye^2	Position cm^{-1}	$S_{mea} \times 10^{28}$ $cm^{-1}/(cm^{-2}$ mole)	$Pos_{Mea.}-Pos_{Cal}$ $\times 10^{-3}$ cm^{-1}	%[a]	$\lvert R\rvert^2_{obs} \times 10^{12}$ Debye^2
0						12341.7834	0.76	0.9	9.4	4.27
2	12339.4432	1.48	2.2	8.1	4.21	12343.2074	1.99	1.2	−2.5	3.77
4	12337.7433	2.44	0.3	−8.4	3.57	12344.5194	3.27	−0.9	−1.0	3.83
6	12335.9334	3.50	−1.9	−8.6	3.55	12345.7241	4.03	−0.4	−10.0	3.51
8	12334.0183	4.50	0.5	−6.1	3.63	12346.8189	5.17	0.0	−4.0	3.70
10	12331.9907	5.48	−0.1	−1.1	3.80	12347.8047	6.11	1.3	0.3	3.85
12	12329.8539	5.89	−0.2	−3.1	3.72	12348.6777	6.27	−0.1	−5.0	3.65
14	12327.6077	6.42	0.0	0.8	3.85	12349.4423	6.71	0.0	−1.7	3.75
16	12325.2500	6.22	−.16	−3.7	3.67	12350.0970	6.92	0.4	1.0	3.83
18	12322.7843	6.14	−1.4	−3.0	3.68	12350.6404	6.49	−0.3	−2.9	3.67
20	12320.2110	6.04	0.9	0.3	3.78	12351.0730	7.18	−1.4	11.9	4.27
22	12317.5251	6.10	0.5	8.3	4.09	12351.3975	6.41	−0.2	8.7	4.09
24	12314.7321	5.78	2.9	12.1	4.24					
26	12311.8248	4.34	0.8	−3.8	3.57					
28	12308.8095	3.99	0.9	2.1	3.75	12351.7055*	8.90	1.7	54.6	8.06
30	12305.6846	3.50	1.3	5.1	3.84	12351.5843*	4.56	0.1	24.8	4.83
32	12302.4481	2.86	0.5	3.4	3.74	12351.3534	2.59	0.0	−10.0	3.27
34	12299.1020	2.35	0.2	3.8	3.73					
36	12295.6453	1.69	−0.2	−6.8	3.33	12350.5581*	2.22	0.1	16.4	4.23
38	12292.0775	1.38	−1.2	−3.1	3.41	12349.9922*	1.65	−1.0	11.6	3.96
40	12288.4010	1.08	−0.3	−1.6	3.42	12349.3168*	1.66	0.4	32.3	5.11
42	12284.6117	0.94	−1.6	11.4	3.88	12348.5267*	1.43	−1.1	40.6	5.76
44						12347.6243*	0.93	−2.6	32.3	4.99
46	12276.7050	0.39	0.7	−16.3	2.89	12346.6132*	0.55	−0.7	16.0	3.97
48	12272.5848	0.32	1.7	−0.5	3.30	12345.4884*	0.52	0.2	36.6	5.19

[a] Intensity ratio of the difference and measured intensity; the blended lines are marked with *.

intensities are described only by the principal effective dipole moment parameters $M^{|\Delta\ell_2|}_{\Delta V}$.

Using the approach described above, we have performed the least-squares fittings of the experimental line intensities for three $^{13}C^{16}O_2$ bands near 806 nm. The values of the expansion coefficients ${}^{J}C^{V_1V_2\ell_2V_3}_{PN\varepsilon}$ of the eigenfunctions have been obtained from the global fit of the effective Hamiltonian parameters to the observed line positions. We used the same sample of effective Hamiltonian parameters as in Ref. [17]. The partition function $Q(T)$ and nuclear statistical weights were taken from Ref. [18]. Two effective dipole moment parameters $M_{1\,0\,5}$ and $M_{0\,2\,5}$ were fitted to the observed line intensities, which were weighted according to the estimated accuracy 4% and 10% for the lines of the cold bands and the 11151–01101 hot band, respectively. The blended lines marked with '*' in Tables 1 and 2 were excluded from the fit. In addition, a few weak lines with large residuals were also excluded from the fit. The weighted standard deviation of the fit is 1.04 and RMS of the residuals is 5.09%. The values of these parameters are presented in Table 5. For comparison, the corresponding effective dipole moment parameters for $^{12}C^{16}O_2$ isotopologue are also presented in Table 5, which were retrieved by fitting the line intensities of the same bands of $^{12}C^{16}O_2$ given in Ref. [4].

Fig. 4 shows the residuals between the measured and calculated line intensities of $^{12}C^{16}O_2$ and $^{13}C^{16}O_2$ transitions belonging to $P=17$ series. Note that only the residuals for the line intensities involved in the global fit are plotted in this figure.

4. Discussion and conclusion

In Fig. 5, we give the comparison of the line positions measured in this work to those measured by ICLAS [5]. The declared accuracy of ICLAS measurement is 0.01 cm^{-1}, about three times worse than the present study. But the discrepancy in line positions between the ICLAS and CRDS values vary from 0.01 to 0.04 cm^{-1}. It can be a result of the spectral calibration. The ICLAS spectrum was calibrated with the atmospheric water line positions given in the HITRAN96 database [19], where the air induced line shifts have not been considered. The air induced line shifts of the water lines vary from −0.005 to −0.035 cm^{-1} (at 1 atm) in the 12,315–12,470 cm^{-1} region according to the HITRAN2008 database [20]. As a result, the ICLAS line positions may be larger than the true values. Fig. 5 also presents the comparison between our values and the calculated values given in the CDSD databank. Those calculations were performed within the framework of the method of effective operators based on the set of the effective Hamiltonian parameters [21], which was determined from the global fit to the observed line positions collected from the literatures including the ICLAS data from Ref. [22]. The difference is less than 0.01 cm^{-1} for majority of the lines. The new observed line positions will allow us to improve the set of effective Hamiltonian parameters.

The comparison between the measured line intensities of $^{13}C^{16}O_2$ and those listed in the CDSD databank is given in Fig. 6. The line intensities of the strongest band 10051–

Table 3
Line parameters of the 11151–01101 band of $^{13}C^{16}O_2$.

J	P(J)				R(J)			
	Position cm^{-1}	$S_{mea} \times 10^{28}$ cm^{-1}/(cm^{-2} molecule)	$Pos_{Mea.}-Pos_{Cal}$ $\times 10^{-3}$ cm^{-1}	$\|R\|^2_{obs} \times 10^{11}$ $Debye^2$	Position cm^{-1}	$S_{mea} \times 10^{28}$ cm^{-1}/(cm^{-2} molecule)	$Pos_{Mea.}-Pos_{Cal}$ $\times 10^{-3}$ cm^{-1}	$\|R\|^2_{obs} \times 10^{11}$ $Debye^2$
3	12407.7531	0.32	−2.7	1.61	12413.0138	0.63	2.4	2.24
4	12406.8808	0.41	0.2	1.49	12413.6499	0.69	0.6	1.95
5	12405.9797	0.58	−0.8	1.67	12414.2379	0.75	−1.5	1.79
6					12414.8151	0.77	−3.7	1.60
7	12404.0836	0.64	−0.2	1.35	12415.3472	0.73	1.6	1.34
8	12403.0811	0.76	−0.8	1.46	12415.8633	0.81	−3.5	1.37
9	12402.0657	0.99	0.2	1.73	12416.3303	0.91	0.1	1.44
10	12400.9971	0.95	−3.3	1.55	12416.7924	0.86	−0.6	1.27
11	12399.9252	1.02	−0.6	1.58	12417.1936	1.11	0.4	1.56
12	12398.7963	1.12	−1.1	1.66	12417.5982	1.09	0.5	1.49
13	12397.6655	1.15	0.8	1.64	12417.9341	1.21	−0.2	1.60
14	12396.4729	1.15	−0.2	1.62	12418.2810	1.34	0.4	1.75
15	12395.2835	1.42	1.3	1.97	12418.5539	1.32	0.1	1.71
16	12394.0280	1.05	0.5	1.45	12418.8428	1.22	0.8	1.58
17	12392.7785	1.14	0.1	1.58				
18	12391.4616	1.18	1.0	1.65	12419.2817	1.16	−0.1	1.54
19	12390.1539	1.00	0.6	1.42	12419.4277	1.06	−0.2	1.44
20	12388.7723	1.07	−0.5	1.57	12419.6001	1.12	0.1	1.55
21	12387.4067	1.07	−0.5	1.61				
22	12385.9653	1.33	1.4	2.08	12419.7961	0.68	−0.9	1.02
23					12419.8154	1.00	−0.1	1.55
24	12383.0352	1.03	1.1	1.76	12419.8703	0.67	−2.1	1.11
25	12381.5513	0.91	−0.2	1.64				
26	12379.9814	1.03	−2.1	1.99				
27					12419.7148	0.85	−1.8	1.67
28	12376.8079	0.89	−4.3	1.95	12419.6593	0.45	−0.1	0.95
30	12373.5207	0.75	0.2	1.92	12419.3730	0.69	1.9	1.71
32	12370.1085	0.54	0.2	1.67	12418.9640	0.53	2.3	1.56
33	12368.3866	0.60	−2.8	2.02	12418.6578	0.54	0.8	1.77
34	12366.5766	0.45	0.7	1.69	12418.4259	0.70	−5.5	2.53
35					12418.0603	0.38	−0.7	1.51
36	12362.9263	0.47	2.8	2.19	12417.7772	0.34	−3.0	1.53
37					12417.3420	0.25	−1.5	1.23
38	12359.1496	0.17	−1.5	1.01	12417.0050	0.16	−3.3	0.88
39	12357.2530	0.18	1.7	1.16	12416.5027	0.17	−2.2	1.07
40	12355.2636	0.079	4.7	0.59	12416.1162	0.12	0.4	0.89
41	12353.2920	0.12	−5.9	1.00	12415.5461	0.13	1.1	1.03
43	12349.2255	0.21	1.1	2.29	12414.4634	0.11	−0.7	1.22
45					12413.2612	0.072	−0.8	1.05

Table 4
Spectroscopic parameters (in cm^{-1}) of the rovibrational bands of $^{13}C^{16}O_2$ in the region 12272–12463 cm^{-1}.

Lower state	G_v	B_v	$D_v \times 10^7$								
00001	0.0	0.39023754	1.33346								
01101e	648.47803	0.39061133	1.35489								
01101f	648.47803	0.39124542	1.36377								
Bands	ΔG_v[a]	G_v	B_v	$D_v \times 10^7$	J_{max}[b]	P/R	n/N[c]	RMS[d]	$\|R_0\|^2 \times 10^{11}$	A_1[e]	$A_2 \times 10^5$	RMS[f]
10052–00001	12341.02941(26)	12341.02941(26)	0.37652406 (68)	1.5395(31)	48/48		42/45	0.89	1.671(12)	0.0	−1.34(32)	2.6
10052–00001[A]		*12341.058(6)*	*0.37643(4)*	*0.6(6)*			*19/22*	*10.0*				
10051–00001	12452.59502(22)	12452.59502(22)	0.37476222(39)	1.1883(13)	58/58		53/55	0.81	0.3869(59)	0.0	−3.24(90)	5.4
10051–00001[A]		*12452.609(2)*	*0.374662(7)*	*1.16(4)*			*36/40*	*6.7*				
11151e–00001e	12410.19065(34)	13058.66868(34)	0.3754092(11)	1.2378(55)	43/45		27/32	0.89				
11151f–00001f	12410.19302(44)	13058.67105(44)	0.3760408(15)	1.1590(92)	40/40		26/36	0.96				

Note: The lower state constants were fixed at the values of Ref. [11]. The uncertainties are given in parentheses in the unit of the last quoted digit. In the case of previously analyzed bands, the corresponding spectroscopic parameters are given in italics for comparison: Campargue et al. [5]. $|R_0|^2$ parameters are given in $Debye^2$.

[A] A_1 and A_2 parameters are dimensionless.

[a] Difference between the upper and lower vibrational term values.

[b] J_{max} is the maximum value of the angular momentum quantum number observed for P/R branches.

[c] n: Number of transitions included in the fit; N: number of assigned rotational transitions.

[d] Root mean square deviation for spectroscopic parameters fit (in 10^{-3} cm^{-1}).

[e] The values of A_1 were fixed to zero.

[f] Root mean square deviation for Herman Wallis intensity fit (in 10^{-13} $Debye^2$).

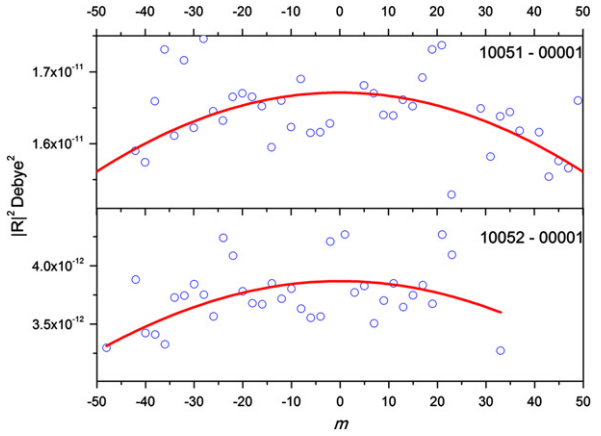

Fig. 3. Experimental (open circles) and calculated (solid lines) transition dipole moments squared of the 10051–00001 and 10052–00001 cold bands of $^{13}C^{16}O_2$. The calculated $|R|^2$ values were obtained using the parameters given in Table 4.

Table 5
Effective dipole moment parameters for $\Delta P=17$ series of transitions in $^{13}C^{16}O_2$ and $^{12}C^{16}O_2$.

$M^{\Delta\ell_2}_{\Delta V_1\Delta V_2\Delta V_3}$ [a]	$^{13}C^{16}O_2$	$^{12}C^{16}O_2$
$M^0_{1\ 0\ 5}$	$-0.40950(76)\times10^{-6}$	$-0.46430(81)\times10^{-6}$
$M^0_{0\ 2\ 5}$	$0.1525(30)\times10^{-7}$	$0.1951(38)\times10^{-7}$

[a] The values of the parameters are given in Debye.

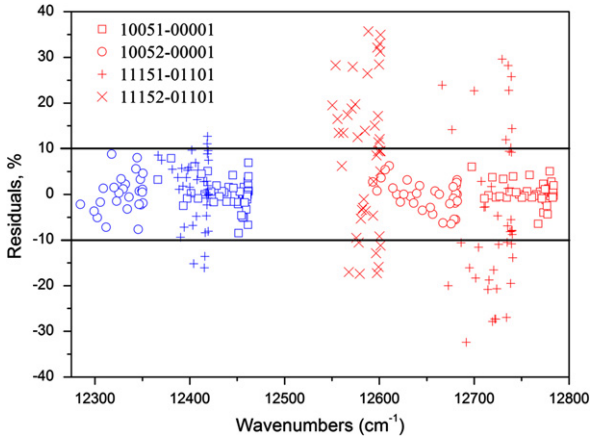

Fig. 4. Residuals between observed and calculated line intensities of $^{12}C^{16}O_2$ (wavenumber over 12,500 cm^{-1}) and $^{13}C^{16}O_2$ (wavenumber below 12,500 cm^{-1}) transitions belonging to $\Delta P=17$ series.

00001 agree within 10%. But the calculated line intensities of the 10052–00001 band contained in the CDSD are about 35% higher than the experimental values. Though the effective dipole moment parameters are mass dependent, the difference between effective dipole moment parameters of different symmetric isotopologues has been shown to be small for carbon dioxide [23]. The CDSD line intensities for the considered bands of $^{13}C^{16}O_2$ were

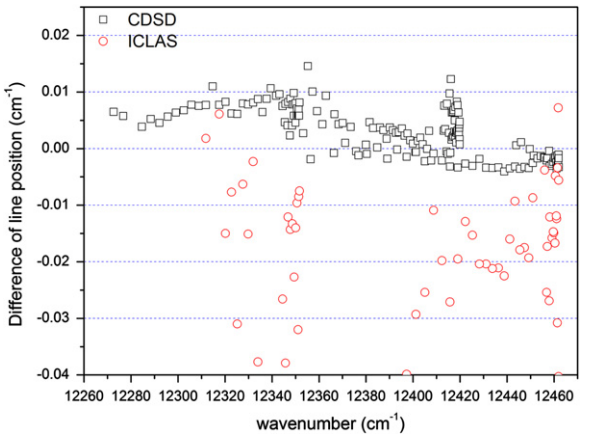

Fig. 5. Difference between the line positions given in this work and those from other studies for $^{13}C^{16}O_2$ near 806 nm. Open Circles: observed line positions by ICLAS [5]. Open Squares: calculated values contained in CDSD [10].

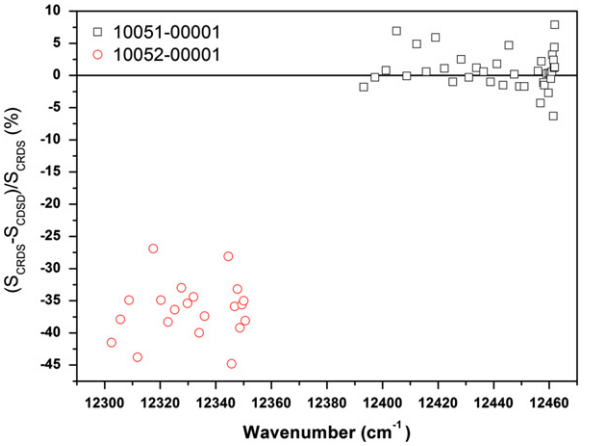

Fig. 6. Comparison of the line intensities for $^{13}C^{16}O_2$ near 806 nm from this work to those contained in CDSD [10].

obtained by the calculations with the effective dipole moment parameters for the principal isotopologue, which were fitted to the band intensities of 10051–00001 and 10052–00001 bands measured by ICLAS and those given in Ref. [24]. However, only one effective dipole moment parameter instead of two necessary parameters has been used to calculate the line intensities of these two bands. The present study implies that the line intensities of the 10052–00001 band are more sensitive to the missed parameter. The HITRAN2008 database [20] includes the line parameters for both studied cold bands of $^{13}C^{16}O_2$ from the atmospheric version of the CDSD databank [10]. The results obtained in this work could be used in the future for the improvement of the line parameters of $^{13}C^{16}O_2$ near 806 nm in the CDSD databank.

Acknowledgements

This work is jointly supported by NSFC (Grant No. 20903085), FRFCU, NKBRSF 2010CB9230 and RFBR-Russia

(Grant No. 06–05–39016). The support of the Groupement de Recherche International SAMIA (Spectroscopie d'Absorption des Molécules d'Intérêt Atmosphérique) between CNRS (France), RFBR (Russia) and CAS (China) is also acknowledged.

References

[1] Battle M, Bender M, Tans PP, White JWC, Ellis JT, Conway T, et al. Global carbon sinks and their variability, inferred from atmospheric O2 and δ13C. Science 2000;287:2467–70.
[2] Ciais P, Denning AS, Tans PP, Berry JA, Randall DA, Collatz GJ, et al. A three-dimensional synthesis study of δ18O in atmospheric CO2. 1. Surface Fluxes. J Geophys Res Atmos 1997;102:5857–72.
[3] Van Herpen MMJW, Ngai AKY, Bisson SE, Hackstein JHP, Woltering EJ, Harren FJM. Optical parametric oscillator-based photoacoustic detection of CO2 at 4.23 μm allows real-time monitoring of the respiration of small insects. Appl Phys 2006;82:665–9.
[4] Song KF, Lu Y, Tan Y, Gao B, Liu AW, Hu SM. High sensitivity cavity ring down spectroscopy of CO2 overtone bands near 790 nm. JQSRT 2011;112:761–8.
[5] Campargue A, Bailly D, Teffo JL, Tashkun SA, Perevalov VI. The v1+5v3 dyad of 12CO2 and 13CO2. J Mol Spectrosc 1999;193: 204–12.
[6] Gao B, Jiang W, Liu AW, Lu Y, Cheng CF, Cheng GS, et al. Ultra sensitive near-infrared cavity ring down spectrometer for precise line profile measurement. Rev Sci Instrum 2010;81:043105.
[7] Lepere M. Line profile study with tunable diode laser spectrometers. Spectrochim Acta, Part A 2004;60:3249–58.
[8] Rautian SG. Sobel'man II, The effect of collisions on the Doppler broadening of spectral lines. Sov Phys Usp 1967;9:701.
[9] Galatry L. Simultaneous effect of Doppler and foreign gas broadening on spectral lines. Phys Rev 1961;122:1218–23.
[10] Perevalov VI, Tashkun SA, CDSD-296 (Carbon dioxide spectroscopic databank): updated and enlarged version for atmospheric applications. In:10th HITRAN database conference, Cambridge MA, USA, 2008. ftp://ftp.iao.ru/pub/CDSD-2008/.
[11] Rothman LS, Hawkins RL, Wattson RB, Gamache RR. Energy levels, intensities, and linewidths of atmospheric carbon dioxide bands. JQSRT 1992;48:537–66.
[12] Chedin A. The carbon dioxide molecule. Potential, spectroscopic, and molecular constants from its infrared spectrum. J Mol Spectrosc 1979;76:430–91.
[13] Teffo JL, Sulakshina ON, Perevalov VI. Effective Hamiltonian for rovibrational energies and line intensities of carbon dioxide. J Mol Spectrosc. 1992;156:48–64.
[14] Perevalov VI, Lobodenko EI, Lyulin OM, Teffo JL. Effective dipole moment and band intensities problem for carbon dioxide. J Mol Spectrosc 1995;171:435–52.
[15] Teffo JL, Lyulin OM, Perevalov VI, Lobodenko EI. Application of the effective operator approach to the calculation of $^{12}C^{16}O_2$ line intensities. J Mol Spectrosc 1998;187:28–41.
[16] Tashkun SA, Perevalov VI, Teffo JL, Tyuterev VG. Global fit of $^{12}C^{16}O_2$ vibrational–rotational line intensities using the effective operator approach. JQSRT 1999;62:571–98.
[17] Perevalov BV, Deleporte T, Liu AW, Kassi S, Campargue A, Auwera JV, et al. Global modeling of $^{13}C^{16}O2$ absolute line intensities from CW-CRDS and FTS measurements in the 1.6 and 2.0 mm regions. JQSRT 2008;109:2009–26.
[18] Fischer J, Gamache RR, Goldman A, Rothman LS, Perrin A. Total internal partition sums for molecular species in the 2000 edition of the HITRAN database. JQSRT 2003;82:401–12.
[19] Rothman LS, Rinsland CP, Goldman A, Massie ST, Edwards DP, Flaud JM, et al. The Hitran molecular spectroscopy database and hawks (Hitran atmospheric workstation). JQSRT 1998;60:665–710.
[20] Rothman LS, Gordon IE, Barbe A, Benner DC, Bernath PF, Birk M, et al. The Hitran 2008 molecular spectroscopic database. JQSRT 2009;110:533–72.
[21] Ding Y, Macko P, Romanini D, Perevalov VI, Tashkun SA, Teffo JL, et al. High sensitivity cw-cavity ring down and Fourier transform absorption spectroscopies of 13CO2. J Mol Spectrosc 2004;226: 146–60.
[22] Weirauch G, Campargue A. Spectroscopy and intensity measurements of the 3v1+3v3 tetrad of $^{12}CO_2$ and $^{13}CO_2$. J Mol Spectrosc 2001;207:263–8.
[23] Karlovets EV, Perevalov VI. Calculation of the carbon dioxide effective dipole moment parameters of the qJ and q^2J types for rare isotopologues. Atmos Oceanic Opt 2011;24:101–6.
[24] Campargue A, Charvat A, Permogorov D. Absolute intensity measurements of CO_2 overtone transitions in the near-infrared. Chem Phys Lett 1994;223:567–72.